ELEVATED TEMPERATURE DEFORMATION BEHAVIORS AND MICROSTRUCTURE EVOLUTIONS OF CAST SA508-4N STEEL*

Xuekun Shang[1]
Xiaowei Du[2]
Xitao Wang[3*]

Abstract

The deformation behaviors under both tensile and compressive forces and microstructure evolutions of cast SA508-4N steel were investigated at elevated temperatures. True stress-strain data were obtained from hot deformation experiments performed on a Gleeble-3500 thermal-simulator under different temperatures (750-1200°C) and strain rates (0.001-10 s^{-1}). The reduction of area decreases as a function of temperature from 750°C to 900°C and then increases. At 1200°C, the reduction of area reaches more than 99% with the strain rates of 0.5 s^{-1} and 1.0 s^{-1}. The dynamic recrystallization under compressive stress occurs at 800°C under low strain rate and a complete dynamic recrystallization can be observed when the temperature reaches above 1100°C. A “two-stage” flow stress constitutive model concerned with dynamic recovery and dynamic recrystallization was established based on the true stress-strain data. This model shows good agreement with experiment results. Moreover, we developed a dynamic recrystallized grain size model to describe the average grain size after complete dynamic recrystallization.

Keywords: SA508-4N Steel; dynamic recrystallization; constitutive model; hot deformation.

[1] *PhD Candidate, Collaborative Innovation Center of Steel Technology, University of Science and Technology Beijing Institution of work or study, Beijing, PR China.*
[2] *Master, Collaborative Innovation Center of Steel Technology, University of Science and Technology Beijing Institution of work or study, Beijing, PR China.*
[3] *Professor, Innovation Center of Steel Technology, University of Science and Technology Beijing Institution of work or study, Beijing, PR China.*

1 INTRODUCTION

Reactor pressure vessel (RPV) is a critical component in nuclear power plant and required to be able to endure decades of high pressure, high temperature and intense neutron irradiation [1-3]. With the development of larger and more efficient nuclear power plant, conventional RPV materials such as SA508 Gr.3 and SA533 Gr.B become unsuitable for new generation power plant. SA508-4N steel, containing higher Ni and Cr content and lower Mn, is a promising candidate material for RPV of generation IV nuclear power plant due to its excellent strength and toughness [4, 5].

Many investigations have been made to evaluate the mechanical property, irradiation resistance and hot deformation behavior of this steel. Wu et al. compared the critical cleavage fracture stress of SA508-4N and SA508 Gr.3 by using experiments and finite element method (FEM) analysis and found that SA508-4N steel possesses higher strength and notch toughness as well as improved cleavage fracture behavior [3]. Lee et al. found that cleavage fracture is controlled by the initiation of micro-cracks in the carbides and a reduction of coarse carbides near the crack tip can benefit toughness [6]. Moreover, they evaluated the effects of Ni and Cr contents in the SA508-4N steel and found that Ni content was more effective on the impact toughness while Cr content was more effective on the fracture toughness [7]. Park et al. investigated the microstructural changes caused by neutron irradiation of SA508-4N and found that Ni is not the controlling factor in the irradiation damage behavior and the Mn content of the steel is a dominant factor in the irradiation-induced microstructural development of solute-related hardening features [8]. Liu et al performed hot deformation experiments and obtained the hot processing map of SA508-4N steel [9]. Sun et al. established a flow stress constitutive model based on the deformation data of SA508-3 steel and represented a successful application in forging process, the dynamic recovery (DRV) and dynamic recrystallization (DRX) process were also discussed [10]. However, very few works have been reported about the flow stress behavior based on the basics of the microstructure evolution affected by DRV and DRX. In this work, we focused on the both tensile and compression deformation behavior as well as mechanical property of the SA508-4 steel. The influence of DRX and DRV were considered to establish flow stress constitutive model and the relationship between microstructure evolution and deformation parameters such as strain, strain rate, temperature was discussed.

2 MATERIAL AND METHODS

The chemical composition of SA508-4N steel used in this study is as follows (wt. %): 0.23C-0.317Mn-0.0059P-0.0037S-0.157Si-3.62Ni-1.8Cr-0.51Mo-0.0051Cu-(bal.)Fe. Cylindrical specimens with 10mm in diameter and 121.5mm in height were used for the isothermal hot tensile tests on a Gleeble-3500 thermal-mechanical stimulator following the procedure shown in Figure 1a. The specimens were heated to 1250°C with a rate of 5°C/s and held for 1min to avoid thermal gradients and make the microstructures uniformity. Subsequently, the specimens were cooled down to the temperatures of 750°C, 800°C, 900°C, 1000°C, 1100°C and 1200°C at a rate of 5°C/s and held for 10s, following with tensile tests at the strain rates of $0.1s^{-1}$, $0.5s^{-1}$ and $1s^{-1}$. After fracture, the specimens were quenched into cold water to preserve the microstructures. In order to get more information about the influence of strain rate on the hot deformation behaviors of SA508-4N steel, additional tensile tests with strain rates $0.01s^{-1}$, $0.05s^{-1}$ and $5s^{-1}$ were performed at the temperature of 1000°C. Similarly, isothermal hot compression tests were also performed on the same stimulator

according to the procedure in Figure 1b using cylindrical specimens with 8mm in diameter and 12mm in height. Different compression tests temperatures of 700°C, 800°C, 900°C, 1000°C, 1100°C and 1200°C and strain rates of $0.01s^{-1}$, $0.01s^{-1}$, $0.1s^{-1}$, $1s^{-1}$and $10s^{-1}$ were used respectively. All the specimens were compressed to a true strain of 0.7, except that some addition test with different true strains of 0.1, 0.3, 0.5 and 1 at 1000°C under all strain rates mentioned above were performed to figure out the microstructure evaluation process with the increase of strain. Ti foils were used between the sample and die to minimize the friction and possible deformation asymmetry. The true stress-strain curves were automatically recorded during hot deformation. The microstructures during deformation and the fracture morphology were observed by optical microscopy (OM: 55XA) and scanning electron microscopy (SEM) performed on a ZEISS SUPRA 55 Field Emission Scanning Electron Microscope.

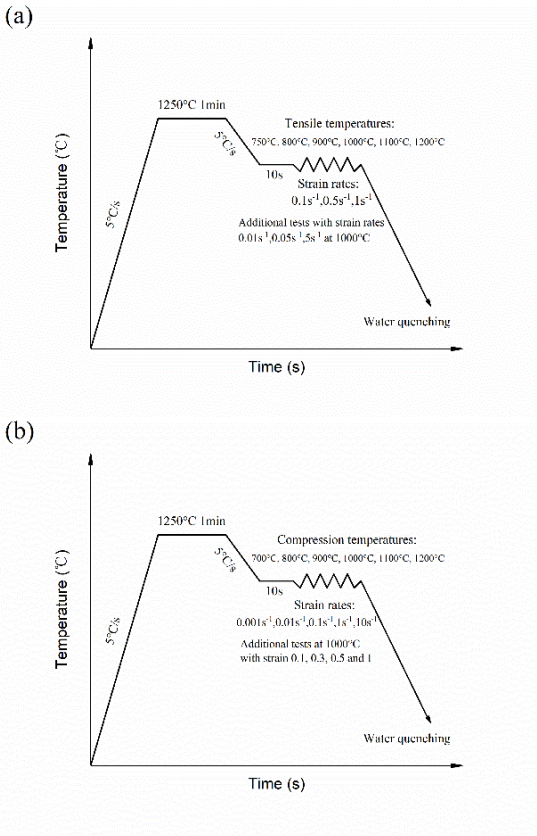

Figure 1. Hot deformation procedures for: (a) tensile experiments and (b) compression experiments.

3 RESULTS AND DISCUSSION

3.1 Tensile flow behavior and fracture morphology

Figure 2 shows the true tensile stress-strain curves of cast SA508-4N steel under different temperatures and strain rates. It is obvious that the values of true stress decrease with the growth of temperature and the drop of strain rate. Rapidly decline of true stress before fracture can be noticed with the temperature of 900°C and below or a strain of $5s^{-1}$, indicating that SA508-4N steel shows good ductility when the temperature exceed 900°C at the strain rates of 0.01-$1s^{-1}$.

Figure 3 shows the fracture morphologies of cast SA508-4N steel under the temperatures of 750°C, 800°C, 900°C, 1000°C, 1100°C and 1200°C at strain rates $0.1s^{-1}$, $0.5s^{-1}$ and $1s^{-1}$. At the temperatures of 750°C and 800°C, the fracture surfaces, which correspond to SEM images Figure 3(a-f), are characterized by dimples, indicating ductile tensile fracture. Both cleavages and fine dimples are observed at the temperature of 900°C. Moreover, the dimples become smaller and the cleavage feature dominates with the increased strain rate, as shown in Figure 3(g-i). This mixture morphology of transgraular fracture and intergranular fracture maybe the sign of a reduction of ductility at this temperature.

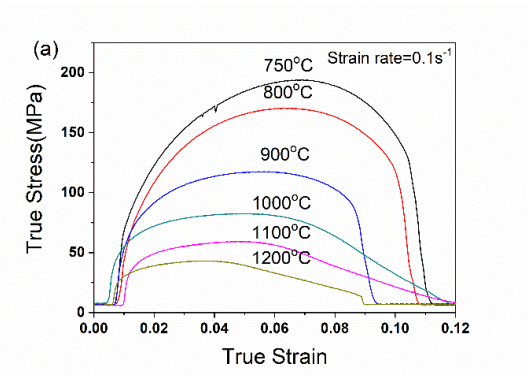

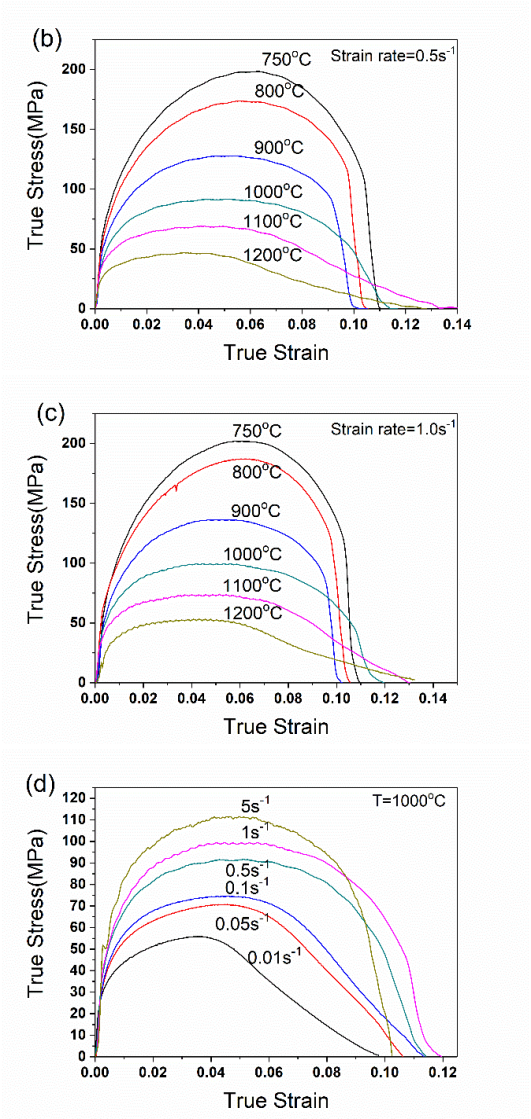

Figure 2. True tensile stress-strain curves of cast SA508-4N steel in different temperatures at the strain rates (a) $0.1s^{-1}$, (b) $0.5s^{-1}$, (c) $1.0s^{-1}$ and (d) at different strain rates in the temperature of 1000°C.

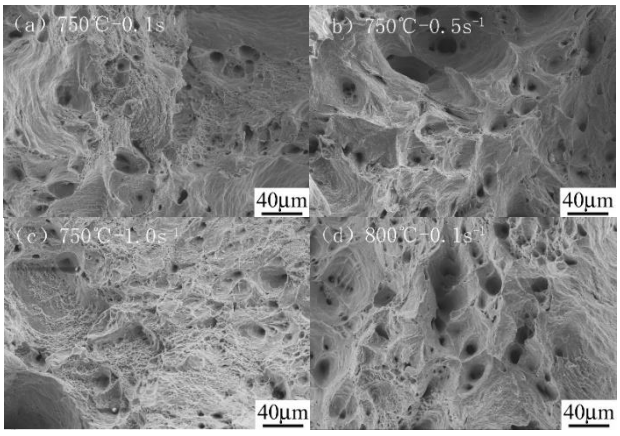

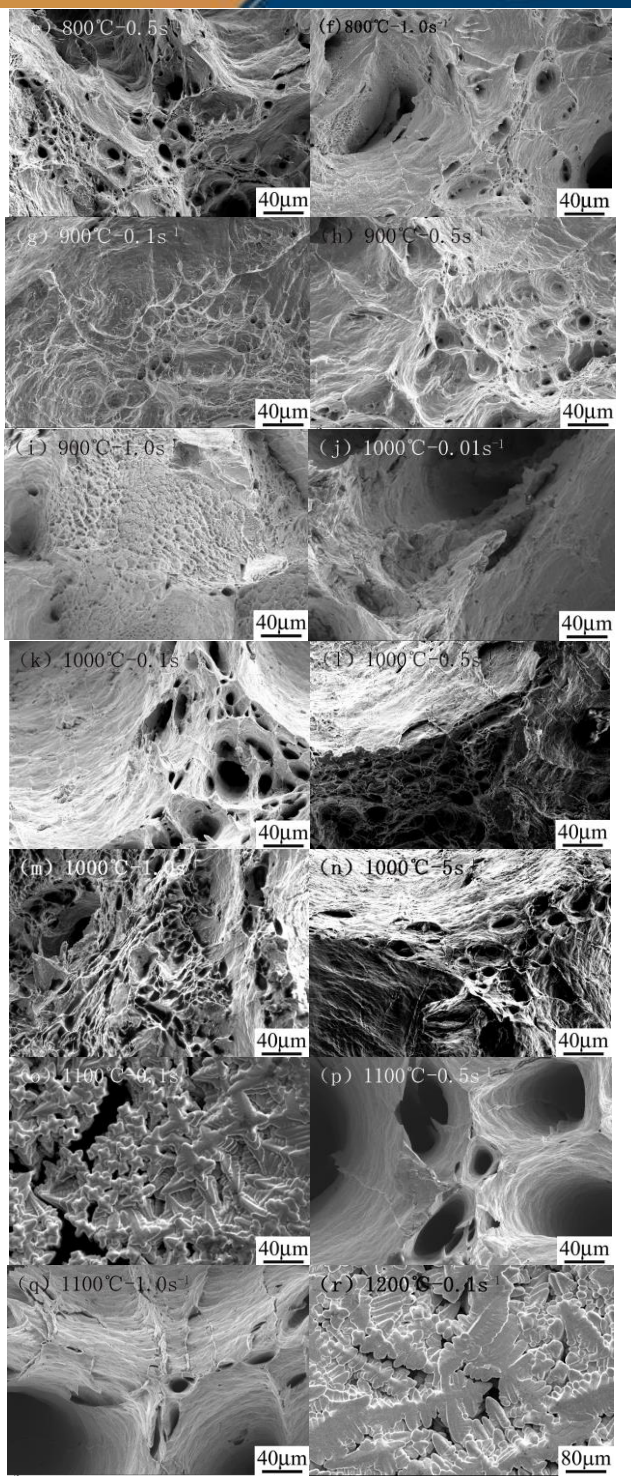

Figure 3. Microscopic fracture morphologies of cast SA508-4N steel under different temperatures (750°C, 800°C, 900°C, 1000°C, 1100°C and 1200°C) and strain rates ($0.1s^{-1}$, $0.5s^{-1}$, $1s^{-1}$).

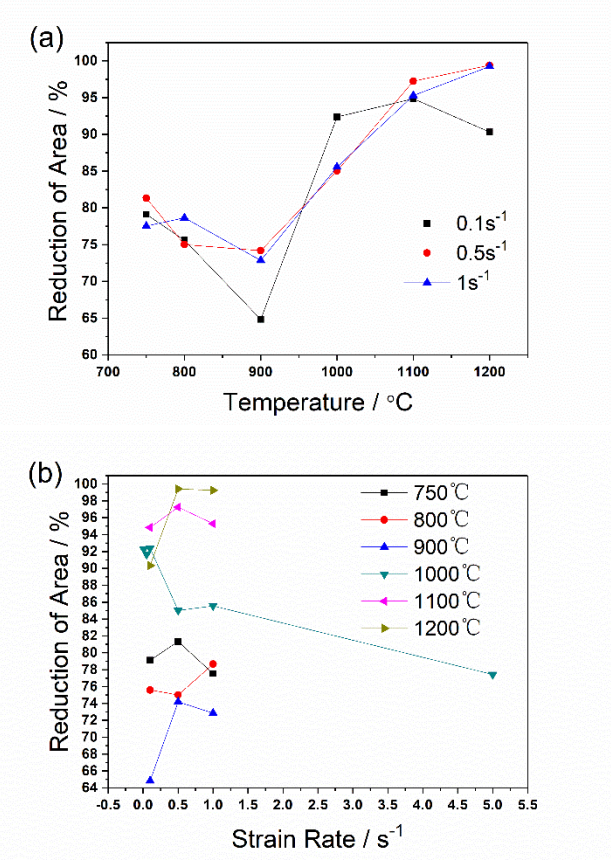

Figure 4. Reduction of area values obtained from tensile tests.

Large, deep dimples can be found in Figure 3(j-n,p,q) probably due to the growth and coalescence of the voids at the temperatures of 1000°C and 1100°C. As shown in Figure 3(o,r), with a strain rate of $1s^{-1}$ at 1100°C and 1200°C, the fracture surfaces characterize with columnar crystals because rupture fracture occurred during deformation and the fracture zone of the steel melted when electric current flowed through a very thin junction.

Figure 4 depicts the reduction of area values of cast SA508-4N steel under different temperatures and strain rates. The reduction of area values decreases as a function of temperature from 750°C to 900°C and then increases. Clearly, temperature has more influence than strain rate on the ductility of the steel here. At 1200°C, the reduction of area reaches more than 99% with the strain rates of 0.5 s^{-1} and 1.0 s^{-1}, this rupture fracture is common at high temperature where it is often associated with dynamic recrystallization. Under the temperature of 900°C, the formation of voids when deformation may lead to the brittle feature of the steel without or with limited dynamic recrystallization and the ductility decrease because of the benefits from the increased temperature to voids formation and growth. When the temperature reach over 900°C, dynamic recrystallization begins to dominate and thus the ductility is enhanced.

3.2 Compression flow behavior and model establishment

Figure 5 shows the compression true stress-strain curves of cast SA508-4N steel in different temperatures under strain rates of $0.01s^{-1}$, $0.01s^{-1}$, $0.1s^{-1}$, $1s^{-1}$and $10s^{-1}$. It is easily checked that working hardening and dynamic softening (dynamic recovery and dynamic recrystallization) effects exist during hot deformation. In general, with a specified temperature, the flow stress increases with higher strain rates; with a specified strain rate, the flow stress decreases with higher temperatures[11]. The strain hardening rate, defined as $\boldsymbol{\theta} = \frac{\partial \sigma}{\partial \varepsilon}$, is used to reveal if dynamic recrystallization occurs [12-14]. As shown in Figure 6 the inflection point is believed to be related to the occurrence of dynamic recrystallization and some important values can be derived from this curve [10,15,16], such as peak stress, critical stress and saturated stress. In general, the relationship between strain hardening rate and stress consisted of three stages: (i) The hardening rate decreases with the flow stress due to the gradually increasing dynamic recovery. (ii) Then the curve changes to a lower slope as the formation of subgrain structure. (iii) At the point where $\frac{\partial^2 \theta}{\partial \sigma^2} = \mathbf{0}$ (inflection point), dynamic recrystallization is believed to occur and the stress is the critical stress $\boldsymbol{\sigma_c}$, Then the strain hardening value drop down to zero at the peak stress $\boldsymbol{\sigma_p}$, indicating the equilibrium between working hardening

and dynamic softening. With the burst of dynamic recrystallization, the value of $\boldsymbol{\theta}$ goes to negative and then back to zero, at which point a steady state is achieved and with the steady state of stress $\boldsymbol{\sigma_{ss}}$. Thus, the critical stress $\boldsymbol{\sigma_c}$, peak stress $\boldsymbol{\sigma_p}$ and steady state stress $\boldsymbol{\sigma_{ss}}$ and corresponding strains can be calculated from Figure 6.

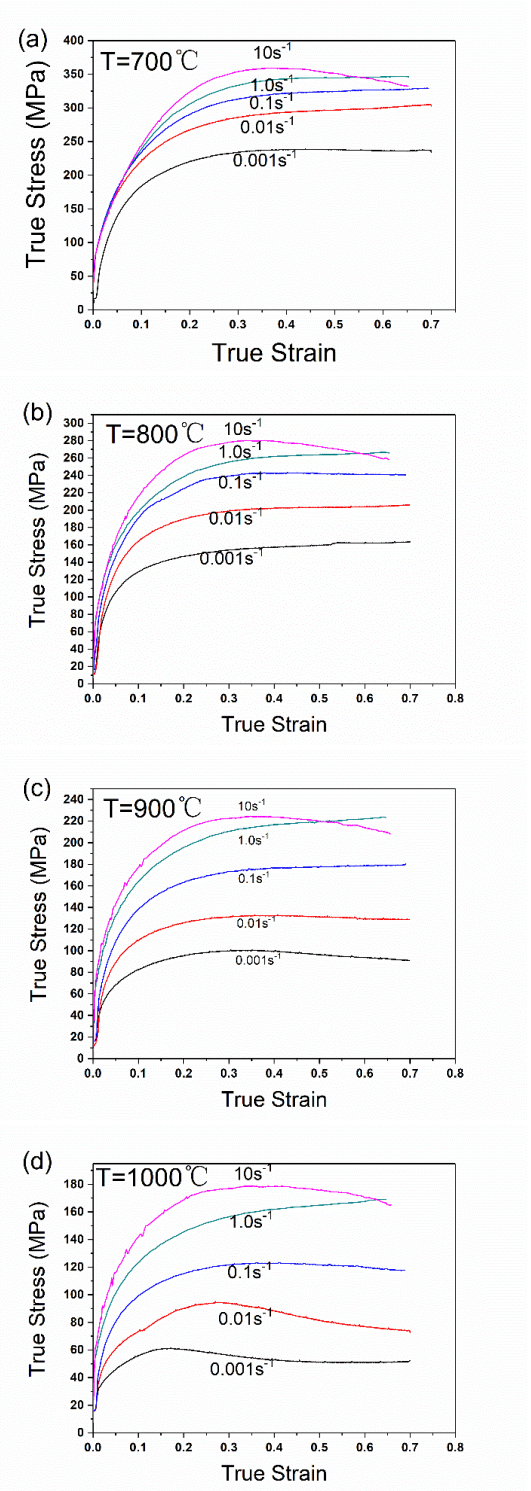

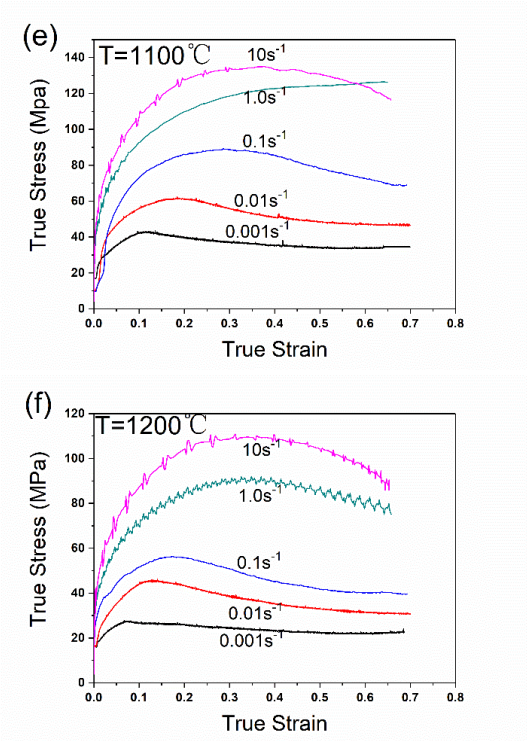

Figure 5. True compression stress-strain curves of cast SA508-4N steel in temperatures at (a) 700°C, (b) 800°C, (c) 900°C, (d) 1000°C, (e) 1100°C and (f) 1200°C under strain rates of 0.01s^{-1}, 0.01s^{-1}, 0.1s^{-1}, 1s^{-1}and 10s^{-1}.

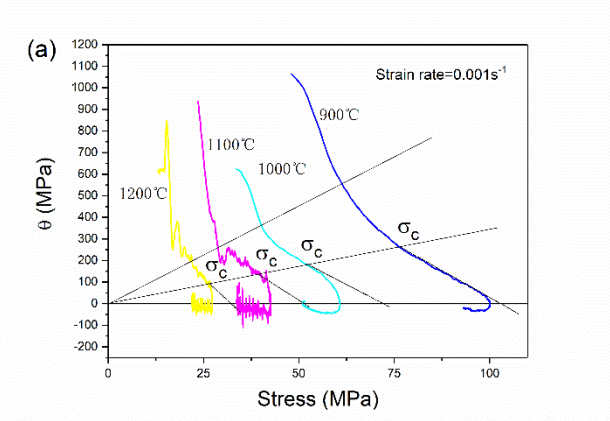

Figure 6. Relationships between (a) strain hardening rate $\boldsymbol{\theta} = \frac{\partial \sigma}{\partial \varepsilon}$ and stress at different temperatures under the strain rate of 0.001s^{-1}.

Using the method above and the compression tests data of cast SA508-4N steel, the values of the critical strain $\boldsymbol{\sigma_c}$ and peak strain $\boldsymbol{\sigma_p}$ at the temperature of 1000°C, 1100°C and 1200°C with strain rates of 0.001s^{-1} to 10s^{-1} were calculated, as shown in Table 1. Therefore, the

normalized strain $\boldsymbol{\varepsilon_c/\varepsilon_p}$ of cast SA508-4N can be observed from a liner fitting with the data in Table 1, as a value of 0.416.

Table 1. Values of critical strain $\boldsymbol{\sigma_c}$ and peak strain $\boldsymbol{\sigma_p}$ under different temperatures and strain rates calculated from compression tests data of cast SA508-4N steel

	1000°C		1100°C		1200°C	
$\dot{\varepsilon}$	ε_c(%)	ε_p(%)	ε_c(%)	ε_p(%)	ε_c(%)	ε_p(%)
0.001s^{-1}	8.01	16.65	7.32	11.37	4.76	7.13
0.01 s^{-1}	15.77	26.02	10.93	17.37	4.85	11.88
0.1 s^{-1}	14.95	32.18	13.17	26.9	9.24	17.80
1.0 s^{-1}	19.36	41.79	17.25	37.87	14.64	28.97
10 s^{-1}	17.37	35.19	16.27	33.62	15.23	29.44

On the basis that dynamic recrystallization occurs after the critical strain during hot deformation, we adopt a "two-stage" constitutive model to predict the flow behavior of the cast SA508-4N steel. The flow stress can be given by [10,14,17-19],

$$\begin{cases} \sigma = [\sigma_{sat}^2 + (\sigma_0^2 - \sigma_{sat}^2)e^{-\Omega\varepsilon}]^{0.5} & (\varepsilon < \varepsilon_c) \\ \sigma = \sigma_{sat} - (\sigma_{sat} - \sigma_{ss})\left[1 - exp\left[-k\left(\frac{\varepsilon-\varepsilon_c}{\varepsilon_p}\right)^n\right]\right] & (\varepsilon \geq \varepsilon_c) \end{cases} \quad (1)$$

where σ is the flow stress, ε the strain, ε_c the critical strain, ε_p the peak strain, σ_{sat} the saturated stress, σ_{ss} the flow stress in steady state and σ_0 the yield stress. After a series of calculation and liner fitting method, the "two-stage" constitutive model was established. The constants in the models are as follows,

$$Z = \dot{\varepsilon}\exp\left(\frac{407.34\ \mathrm{kJ/(mol\cdot K)}}{RT}\right);$$

$$\sigma_p = 100.0 \cdot sinh^{-1}(0.00351 \cdot Z^{0.1670});$$

$$\sigma_0 = 100.0 \cdot sinh^{-1}(0.0223 \cdot Z^{0.08248});$$

$$\sigma_c = 100.0 \cdot sinh^{-1}(0.00377 \cdot Z^{0.1479});$$

$$\sigma_{sat} = 100.0 \cdot sinh^{-1}(0.00450 \cdot Z^{0.1490})$$

$$\sigma_{ss} = 100.0 \cdot sinh^{-1}(0.00254 \cdot Z^{0.1477});$$

$$\Omega = 670.75Z^{-0.0989};$$

$$\varepsilon_p = 0.6162 \cdot Z^{0.09414};$$

$$\varepsilon_c = 0.418\varepsilon_p;$$

k=1.527，n=0.694

To evaluate the practicality of this model, a comparison has been made between the predicted and experimental stress values, as shown in Figure 7. It can be seen that the data predicted by this constitutive model agrees well with the experimental data.

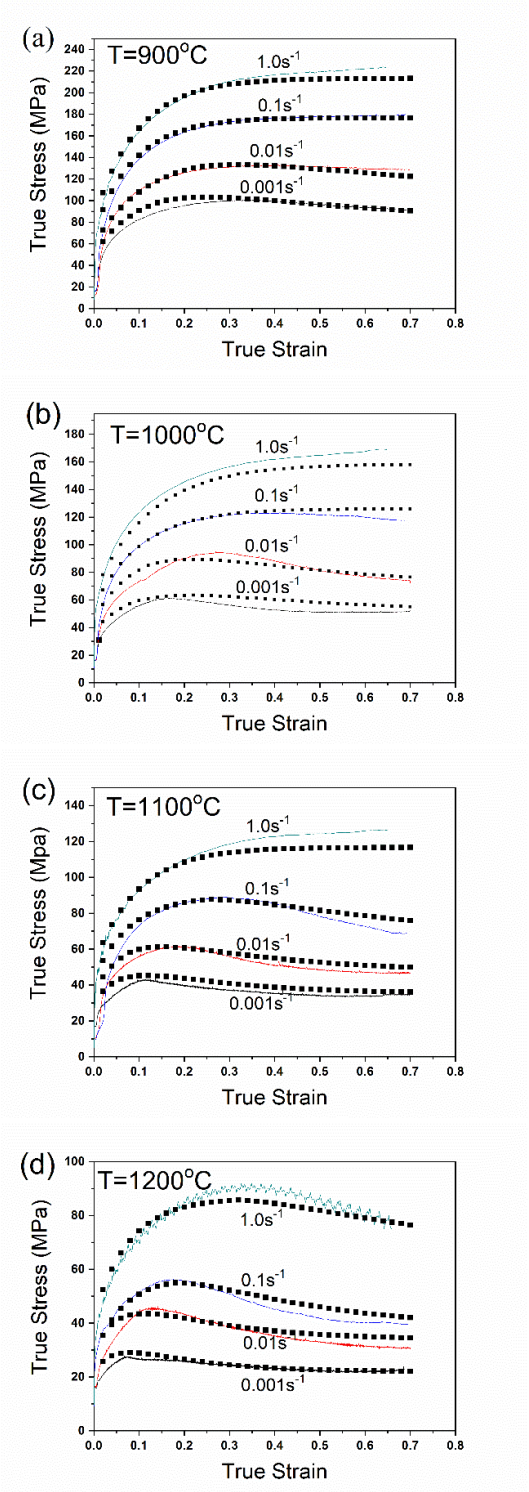

Figure 7. Comparison of experimental and predicted stress values at temperatures of (a) 900°C, (b) 1000°C, (c) 1100°C and (d) 1200°C

3.3 Microstructure evolutions during hot compression tests

Figure 8, Figure 9, Figure 10, Figure 11, Figure 12 and Figure 13 depict selected microstructures of deformed specimens at the temperature of 700-1200°C by strain rates 0.001-10s^{-1} with a strain of 0.7. With the deformation temperature 700°C, no sign of dynamic recrystallization can be found under all strain rates (Figure 7). DRX nucleation occurs at grain boundary at low strain rate of 0.001s^{-1} and 0.01s^{-1} with the deformation temperature 800°C.

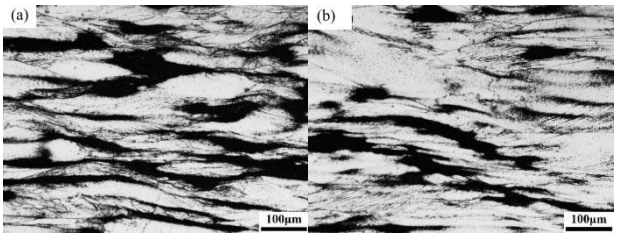

Figure 8. microstructure of deformed specimens at the temperature of 700°C by strain rate of (a) 0.001 s^{-1} and (b) 10 s^{-1} with a true strain of 0.7.

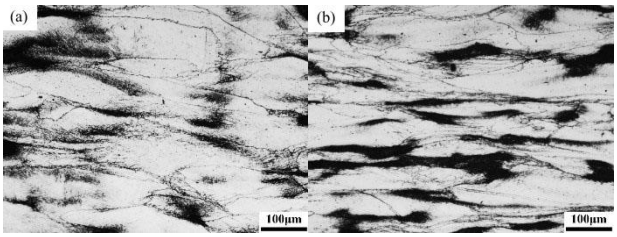

Figure 9. Microstructure of deformed specimens at the temperature of 800°C by strain rate of (a) 0.001 s^{-1} and (b) 0.01 s^{-1} with a true strain of 0.7.

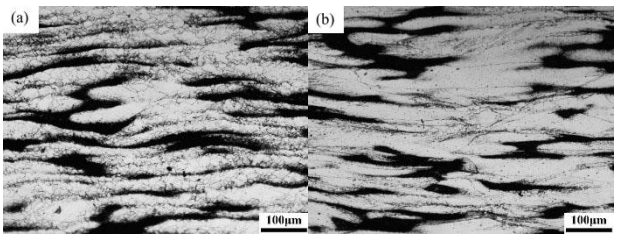

Figure 10. Microstructure of deformed specimens at the temperature of 900°C by strain rate of (a) 0.001 s^{-1} and (b) 10 s^{-1} with a true strain of 0.7.

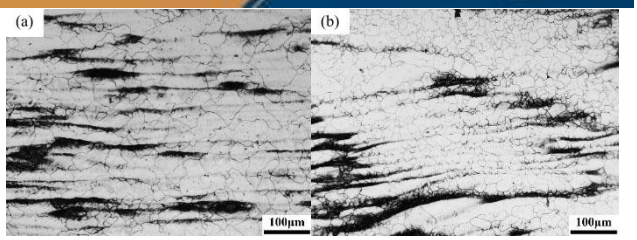

Figure 11. Microstructure of deformed specimens at the temperature of 1000°C by strain rate of (a) 0.001 s^{-1} and (b) 1.0 s^{-1} with a true strain of 0.7.

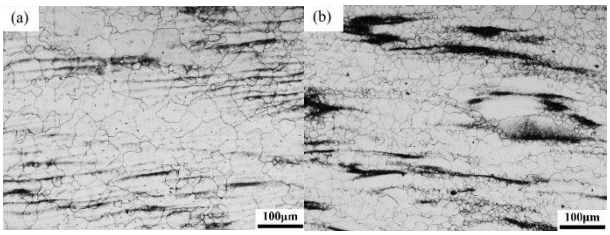

Figure 12. Microstructure of deformed specimens at the temperature of 1100°C by strain rate of (a) 0.01 s^{-1} and (b) 1.0 s^{-1} with a true strain of 0.7.

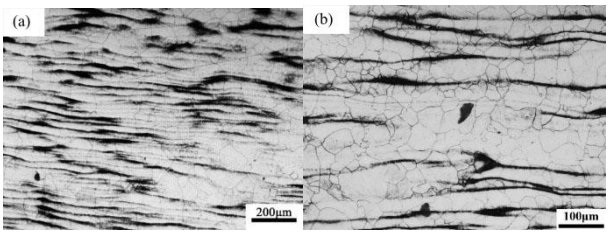

Figure 13. Microstructure of deformed specimens at the temperature of 1200°C by strain rate of (a) 0.1 s^{-1} and (b) 10 s^{-1} with a true strain of 0.7.

At the temperature of 900°C, as shown in Figure 10, partial DRX has been found and the percentage of DRX grains increases as the strain rate decreases, due to a longer time for dislocation annihilation and nucleation and growth of the recrystallized grains. Moreover, over a 90% volume fraction can be observed at the temperature of 1000°C with strain rate 0.01 s^{-1}-10 s^{-1}, and fully DRX has been shown in Figure 11a (1000°C at strain rate 0.001s^{-1}), Fig 12 (1100°C at all strain rates) and Fig13 (1200°C at all strain rates). We can also find that the recrystallized grain size becomes finer as the value of strain rate increases.

Table 2 gives the average diameters of the recrystallized grains of full DRX specimens. As the relationship of the dimensionless Zener-Hollomon parameter (Z) and the fully dynamic recrystallized grain size D_{drx} can be expressed as[10],

$$D_{drx} = \mathrm{A} \cdot Z^{-n} \quad (2)$$

Using the data in Table 2 together with calculation results in section 3.2, we can get the fully dynamic recrystallized grain size model as,

$$\boldsymbol{D_{drx} = 33323 \cdot Z^{-0.1953}} \quad (3)$$

Table 2. Average recrystallized grain size (μm) under different temperatures and strain rates.

	0.001 s^{-1}	0.01 s^{-1}	0.1 s^{-1}	1.0 s^{-1}	10 s^{-1}
1000 °C	47.05	——	——	——	——
1100 °C	117.63	55.95	37.95	23.74	28.99
1200 °C	270.56	135.83	102.50	44.42	45.41

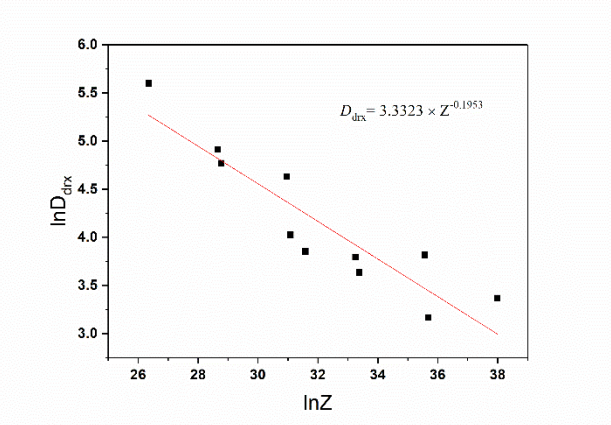

Figure 14. Fitting linearity between the dynamic recrystallized strain size D_{drx} and the Z parameter.

4 CONCLUSION

(1) The ductility of cast SA508-4N steel decreases as temperature increase from 750°C to 900°C and then increases. At 1200°C, the reduction of area reaches more than 99% with the strain rates of 0.5 s^{-1} and 1.0 s^{-1}.

(2) A "two-stage" flow stress constitutive model was established concerned with dynamic recovery and dynamic recrystallization to describe the flow stress behaviors of SA508-4N steel and this constitutive model shows good agreement with experiment results.

(3) The dynamic recrystallization under compressive stress occurs at 800°C under low strain rate with a maximum strain of 0.7 and when the temperature reaches above 1100°C a complete dynamic recrystallization can be observed.

(4) With fully dynamic recrystallized, the average grain size of SA508-4N steel can be expressed as $\boldsymbol{D_{drx} = 33323 \cdot Z^{-0.1953}}$

Acknowledgments

This work was financially supported by the National Natural Science Foundation of China (Grant No. 51601013). This work was also supported by University of Science and Technology (Grant No. 0440001).

REFERENCES

1 Kim MC, Park SG, Lee KH, Lee BS. Comparison of fracture properties in SA508 Gr.3 and Gr.4N high strength low alloy steels for advanced pressure vessel materials. International Journal of Pressure Vessels and Piping. 2015;131:60-6.

2 Yang Z, Liu Z, He X, Qiao S, Xie C. Effect of microstructure on the impact toughness and temper embrittlement of SA508Gr.4N steel for advanced pressure vessel materials. Scientific Reports. 2018;8(1):1-12.

3 Wu S, Jin H, Sun Y, Cao L. Critical cleavage fracture stress characterization of A508 nuclear pressure vessel steels. International Journal of Pressure Vessels and Piping. 2014;123:92-8.

4 Lee KH, Park SG, Kim MC, Lee BS. Cleavage fracture toughness of tempered martensitic Ni-Cr-Mo low alloy steel with different martensite fraction. Materials Science and Engineering A. 2012;534:75-82.

5 Park SG, Kim MC, Lee BS, Wee DM. Correlation of the thermodynamic calculation and the experimental observation of Ni-Mo-Cr low alloy steel changing Ni, Mo, and Cr contents.

Journal of Nuclear Materials. 2010;407(2):126-35.
6 Lee K-H, Kim M-C, Yang W-J, Lee B-S. Evaluation of microstructural parameters controlling cleavage fracture toughness in Mn–Mo–Ni low alloy steels. Materials Science and Engineering: A. 2013;565:158-64.
7 Lee KH, Park Sg, Kim MC, Lee BS, Wee DM. Characterization of transition behavior in SA508 Gr.4N Ni-Cr-Mo low alloy steels with microstructural alteration by Ni and Cr contents. Materials Science and Engineering A. 2011;529(1):156-63.
8 Burke MG, Stofanak RJ, Hyde JM, English CA, Server WL. Microstructural Aspects of Irradiation Damage in A508 Gr 4N Forging Steel: Composition and Flux Effects. Effects of Radiation on Materials: 21st International Symposium. 2008;1(5):194--14.
9 Liu N, Liu Zd, He Xk, Yang Zq, Ma Lt. Hot Deformation Behavior of SA508GR. 4N Steel for Nuclear Reactor Pressure Vessels. Journal of Iron and Steel Research International. 2016;23(12):1342-8.
10 Sun M, Hao L, Li S, Li D, Li Y. Modeling flow stress constitutive behavior of SA508-3 steel for nuclear reactor pressure vessels. Journal of Nuclear Materials. 2011;418(1-3):269-80.
11 Shang X, He A, Wang Y, Yang X, Zhang H, Wang X. Flow Behavior Modeling of a Nitrogen-Alloyed Ultralow Carbon Stainless Steel During Hot Deformation: A Comparative Study of Constitutive Models. Journal of Materials Engineering and Performance. 2015;24(10):4106-18.
12 Mirzadeh H, Cabrera JM, Najafizadeh A, Calvillo PR. EBSD study of a hot deformed austenitic stainless steel. Materials Science and Engineering A. 2012;538:236-45.
13 Poliak EI, Jonas JJ. A one-parameter approach to determining the critical conditions for the initiation of dynamic recrystallization. Acta Materialia. 1996;44(1):127-36.
14 Serajzadeh S, Karimi Taheri A. An investigation on the effect of carbon and silicon on flow behavior of steel. Materials & Design. 2002;23(3):271-6.
15 McQueen HJ, Ryan ND. Constitutive analysis in hot working. Materials Science and Engineering A. 2002;322(1-2):43-63.
16 McQueen HJ, Yue S, Ryan ND, Fry E. Hot working characteristics of steels in austenitic state. Journal of Materials Processing Tech. 1995;53(1-2):293-310.
17 Laasraoui A, Jonas JJ. Prediction of steel flow stresses at high temperatures and strain rates. Metallurgical Transactions A. 1991;22(7):1545-58.
18 He A, Xie G, Yang X, Wang X, Zhang H. A physically-based constitutive model for a nitrogen alloyed ultralow carbon stainless steel. Computational Materials Science. 2015;98:64-9.
19 Serajzadeh S, Taheri AK. Prediction of flow stress at hot working condition. Mechanics Research Communications. 2003;30(1):87-93.